A computational model that predicts reverse growth in response to mechanical unloading

Lik Chuan Lee, Martin Genet, Gabriel Acevedo-Bolton, Karen Ordovas, Julius M. Guccione, Ellen Kuhl

Biomechanics and Modeling in Mechanobiology manuscript No.
(will be inserted by the editor)

A Computational Model that Predicts Reverse Growth in Response to Mechanical Unloading

L.C. Lee · M. Genet · G. Acevedo-Bolton · K. Ordovas · J.M. Guccione · E. Kuhl

Received: date / Revised version: date

Abstract Ventricular growth is widely considered to be an important feature in the adverse progression of heart diseases, whereas reverse ventricular growth (or reverse remodeling) is often considered to be a favorable response to clinical intervention. Over the recent years, a number of theoretical models have been proposed to model the process of ventricular growth while little has been done to model its reverse. Based on the framework of volumetric strain-driven finite growth with a homeostatic equilibrium range for the elastic myofiber stretch, we propose here a reversible growth model capable of describing both ventricular growth and its reversal. We used this model to construct a semi-analytical solution and a numerical solution for reversible growth in an idealized cylindrical tube geometry and a human left ventricular geometry that was reconstructed from magnetic resonance images, respectively. We show that our model is able to predict key features in the end-diastolic pressure-volume relationship that were observed experimentally and clinically during ventricular growth and reverse growth. We also show that the residual stress fields generated as a result of differential growth in the cylindrical tube model are similar to those in other non-identical models utilizing the same geometry.

Keywords Remodeling · Reverse remodeling · Growth · End-diastolic pressure-volume relationship · Finite element method · Magnetic resonance imaging

L.C. Lee, M. Genet, J.M. Guccione
Department of Surgery, School of Medicine, University of California at San Francisco, CA 94143, USA, E-mail: LikChuan.Lee/Julius.Guccione/Martin.Genet@ucsfmedctr.org

G. Acevedo-Bolton, K. Ordvas
Department of Radiology and Biomedical Imaging, School of Medicine, University of California at San Francisco, CA 94143, USA, E-mail: Gabriel.Acevedo-Bolton/Karen.Ordovas@ucsf.edu

E. Kuhl
Departments of Mechanical Engineering, Bioengineering, and Cardiothoracic Surgery, Stanford University, Stanford, CA 94305-4040, USA, E-mail: ekuhl@stanford.edu

1 Introduction

Maladaptive ventricular growth or remodeling[1] is widely considered to be an important determinant of the clinical course of heart failure (Cohn et al. 2000). In its classical form, cardiac remodeling can be categorized into two different types: (1) concentric remodeling with a thickening of the ventricular wall that is induced by an overloading of pressure and (2) eccentric remodeling with a dilation of the ventricles that is induced by an overloading of volume (Grossman et al. 1975). These global geometrical changes in the form of concentric and eccentric remodeling of the heart ventricles are induced microscopically by the parallel and series addition of sarcomere units in the myocytes, respectively. Yet, these two forms of remodeling processes are not mutually exclusive, and can co-exist in other clinical events (e.g. after myocardial infarction) (Opie et al. 2006).

Several theoretical continuum models based on the concept of finite volume growth have recently been proposed to describe ventricular geometrical remodeling (Kroon et al. 2009; Göktepe et al. 2010a,b; Rausch et al. 2011; Kerckhoffs et al. 2012). All these models

[1] In this paper, we used the words "growth" and "remodeling" interchangeably although other authors have used "growth" and "remodeling" to specifically describe a change in mass and properties, respectively.

were developed based upon the concept of the multiplicative decomposition of the deformation gradient tensor into a "growth" and an elastic component. This concept was first applied by Rodriguez et al. (1994) to model tissue growth, and was originally developed by Lee (1969) in the context of finite plasticity. These ventricular growth models were developed with either ventricular myofiber stress as the stimulant of growth (as in Göktepe et al. (2010a,b) and Rausch et al. (2011) for modeling concentric remodeling) or with ventricular myofiber and/or myo-crossfiber strain as the primary stimulant of growth (Kroon et al. 2009; Kerckhoffs et al. 2012).

Although a sizable number of theoretical models have been developed to model the process of ventricular remodeling and to predict the effects clinical treatments have on this process (Klepach et al. 2012), there are little (if any) theoretical models that describe its reversal. Due to the rapid advancement of clinical devices and treatments, reverse remodeling of the ventricles in the form of ventricular size normalization has been observed clinically after some interventions. These treatments include implantation of a left ventricular assist device (Burkhoff et al. 2006), mitral valve repairs (Brinke et al. 2010) and, more recently, bioinjection treatment using calcium-sodium alginate hydrogel (Lee et al. 2013). All of these interventions have been associated with a reduction in ventricular loading due either to a reduction in hemodynamics loading (left ventricular assist devices and mitral valve repairs) or to the presence of mechanical support in the ventricular wall (bioinjection treatment). As such, there is mounting evidence suggesting that a reversal of ventricular remodeling can occur after sufficient and prolonged unloading of the ventricles.

In this paper, we propose a theoretical constitutive model capable of describing both ventricular remodeling and its reversal. The focus here is on pathological ventricular remodeling and reverse remodeling, which is a subset of the broad subject of biological growth and remodeling (Taber 1995; Ambrosi et al. 2011). Our proposed model is based on the generic framework of volumetric strain-driven finite growth described by Göktepe et al. (2010b). The constitutive equations describing reversible ventricular remodeling are given in Section 2. In Sections 3 and 4, we describe the problem formulations for a semi-analytical solution of reversible remodeling in a cylindrical tube model and a numerical solution of reversible remodeling in a realistic human left ventricle model that was reconstructed from magnetic resonance images, respectively. The results from these two models are described in Section 5, where we show the effects of ventricular reverse remodeling (and remodeling) on end-diastolic pressure volume relationship, as well as on the ventricular myofiber stress and strain fields. Finally in Section 6, we discuss the compatibility of our results with clinically and experimentally observed features of ventricular reverse remodeling and remodeling.

2 Methods

2.1 Kinematics of Growth and Reversible Growth

Following Rodriguez et al. (1994) and Göktepe et al. (2010b), we multiplicatively decomposed the deformation gradient $\mathbf{F}$ into an elastic part $\mathbf{F}^e$ and a growth part $\mathbf{F}^g$, i.e.,

$$\mathbf{F} = \mathbf{F}^e \cdot \mathbf{F}^g \ . \tag{1}$$

Without loss of generality, we assumed that the growth tensor $\mathbf{F}^g$ is isotropic. Consequently, $\mathbf{F}^g$ can be parameterized by a scalar growth multiplier θ, i.e.,

$$\mathbf{F}^g = \theta \mathbf{I} \ , \tag{2}$$

where $\mathbf{I}$ is the identity tensor.

Using the definition of an isotropic growth tensor $\mathbf{F}^g$ given in Eq. (2) and the multiplicative decomposition of the deformation gradient given in Eq. (1), the elastic deformation gradient tensor becomes

$$\mathbf{F}^e = \frac{1}{\theta}\mathbf{F} \ . \tag{3}$$

Correspondingly, the elastic part of the right Cauchy stretch tensor and Green-Lagrange elastic strain tensor are then:

$$\mathbf{C}^e = \mathbf{F}^{eT}\mathbf{F}^e, \qquad \text{and} \qquad \mathbf{E}^e = \frac{1}{2}\left(\mathbf{C}^e - \mathbf{I}\right) \ , \tag{4a, b}$$

respectively.

2.2 Elastic Constitutive Model

The elastic deformation of the myocardial tissue is described using a Fung-type transversely isotropic hyperelastic constitutive model with the following strain energy function (Guccione et al. 1991):

$$W(\mathbf{E^e}) = \frac{C}{2}\left(\exp Q - 1\right) \ , \tag{5a}$$

where

$$\begin{aligned} Q =& b_f {E^e_{ff}}^2 + b_s \left({E^e_{ss}}^2 + {E^e_{nn}}^2 + {E^e_{sn}}^2 + {E^e_{ns}}^2 \right) + \\ & b_{fs} \left({E^e_{fs}}^2 + {E^e_{sf}}^2 + {E^e_{fn}}^2 + {E^e_{nf}}^2 \right) . \end{aligned}$$

(5b)

In Eq. (5), C, b_f, b_s and b_{fs} are the material parameters and E_{ij} with $(i,j) \in (f,s,n)$ are the components of the Green-Lagrange strain tensor $\mathbf{E}^e$, which correspond to the material coordinates in the fiber f, sheet s and sheet-normal n directions.

The incompressiblility of the material is enforced by an augmented strain energy function $\hat{W}$

$$\hat{W}(\mathbf{E}^e, p) = W(\mathbf{E}^e) - p(\det\mathbf{F}^e - 1) \ , \tag{6}$$

where p is a hydrostatic pressure that functions as a Lagrange multiplier for the kinematic constraint $\det\mathbf{F}^e = 1$.

The resultant second Piola-Kirchkoff stress tensor is defined as

$$\mathbf{S}^e = \frac{d\hat{W}}{d\mathbf{E}^e} = \frac{dW}{d\mathbf{E}^e} - p\,(\mathbf{C}^e)^{-1} \ , \tag{7}$$

and the Cauchy stress tensor is

$$\boldsymbol{\sigma} = \frac{1}{\det\mathbf{F}^e}\mathbf{F}^e\,\mathbf{S}^e\,\mathbf{F}^{eT} \ . \tag{8}$$

The Cauchy stress enters the equilibrium equation

$$\mathrm{div}\,\boldsymbol{\sigma} = \mathbf{0} \ . \tag{9}$$

where div denotes the divergence with respect to the deformed coordinates and body forces have been neglected.

2.3 Kinetics of Growth

The constitutive model of a reversible growth multiplier is motivated by the strain-driven eccentric growth model proposed by Göktepe et al. (2010b):

$$\frac{d\theta}{dt} = k(\theta)\phi(\lambda_e) \ . \tag{10}$$

In Eq. (10), the evolution of the growth multiplier depends on two scalar functions, namely, a rate limiting scalar function $k(\theta)$ and a growth driving function $\phi(\lambda_e)$ that depends on the elastic myofiber stretch λ_e.

Consistent with the hypothesis that excessive stretch of the myofiber beyond some homeostatic value λ_{h2} can lead to growth and dilation of the ventricles (as in the case when the ventricle is "volume-overloaded"), the functions $k(\theta)$ and $\phi(\lambda_e)$ have the following forms when $\lambda_e \geq \lambda_{h2}$:

$$k(\theta) = \frac{1}{\tau_g}\left(\frac{\theta_{\max} - \theta}{\theta_{\max} - \theta_{\min}}\right)^{\gamma_g} \ , \tag{11a}$$

$$\phi(\lambda_e) = \lambda_e - \lambda_{h2} \ . \tag{11b}$$

Equation (11) is similar to the strain-driven eccentric growth model by Göktepe et al. (2010b). In this equation, γ_g, τ_g, $\theta_{\max}$ and $\theta_{\min}$ are the degree of nonlinearity of sarcomere deposition, a time-scale associated with tissue growth and the prescribed maximum and minimum permissible values of the growth multiplier θ, respectively. If we denote the myofiber direction as $\mathbf{f_0}$, the stretching of the myofiber as a result of growth (or growth stretch) is $\lambda_g = \sqrt{\mathbf{f_0}\cdot\mathbf{F}^{g\,T}\mathbf{F}^g\,\mathbf{f_0}}$. Correspondingly, the elastic myofiber stretch is $\lambda_e = 1/\lambda_g\sqrt{\mathbf{f_0}\cdot\mathbf{F}^T\mathbf{F}\,\mathbf{f_0}}$. It is evident from this equation that growth terminates when either criterion $\theta = \theta_{\max}$ or $\lambda_e = \lambda_{h2}$ is met.

The concept of a homeostatic target value of the myofiber stretch is consistent with the experimental results by Omens (1998), who suggested end-diastolic myofiber strain as the primary stimulus for myocardial growth in volume-overload hypertrophy (instead of end-diastolic stress). This concept is also consistent with the growth models of Kroon et al. (2009), Kerckhoffs (2012) and Taber (2001), although in the latter, myocardial stress (instead of strain) was postulated to be restored to a homeostatic value during growth.

2.4 Kinetics of Reversible Growth

In contrast to Göktepe et al. (2010b) where growth is irreversible, we hypothesize that cardiac growth is reversible in a way that the elastic myocardial stretch λ_e is always normalized to a homeostatic range $\lambda_{h1} \leq \lambda_e \leq \lambda_{h2}$. Consequently, reverse growth occurs when the elastic myofiber stretch is less than the prescribed homeostatic myofiber stretch λ_{h1}. To model reversible growth, we propose the following functional forms for $k(\theta)$ and $\phi(\lambda_e)$ when $\lambda_e \leq \lambda_{h1}$

$$k(\theta) = \frac{1}{\tau_{rg}}\left(\frac{\theta - \theta_{\min}}{\theta_{\max} - \theta_{\min}}\right)^{\gamma_{rg}} \ , \tag{12a}$$

$$\phi(\lambda_e) = \lambda_e - \lambda_{h1} \ . \tag{12b}$$

Similar to Eq. (11), γ_{rg} and τ_{rg} in Eq. (12) are the degree of nonlinearity of sarcomere removal and a time-scale associated with reverse growth, respectively. We also note that reversal of growth terminates when either criterion: $\theta = \theta_{\min}$ or $\lambda_e = \lambda_{h1}$ are met. In addition, the physical limit requires that $\theta_{\min} > 0$.

Last, to ensure that growth does not occur within the homeostatic range of the elastic myofiber stretch, we prescribed $\phi = 0$ when $\lambda_{h1} \leq \lambda_e \leq \lambda_{h2}$.

3 Growth and Reverse Growth of a Cylindrical Tube

To demonstrate the effects of our proposed constitutive model, we constructed a semi–analytical solution of an inflated cylindrical tube undergoing reversible growth in response to changes in the hemodynamics load.

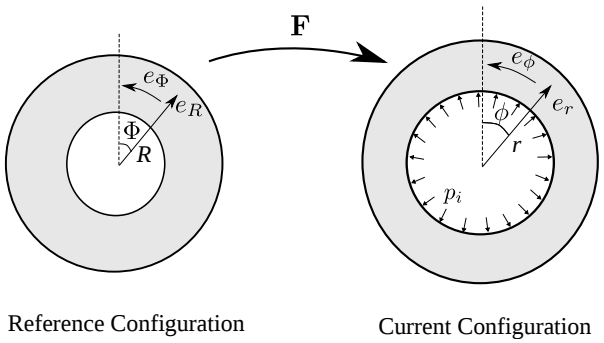

Fig. 1: Inflation of cylindrical tube. The base vectors $\mathbf{e}_z$ and $\mathbf{e_Z}$ point out of the page.

For a cylindrical tube undergoing homogeneous inflation (Figure 1), the deformed radial position r is a function of only the initial radial position R, i.e., $r(R)$ and the resultant deformation gradient tensor is:

$$\mathbf{F} = \frac{dr}{dR}\mathbf{e_r} \otimes \mathbf{e_R} + \frac{r}{R}\mathbf{e}_\phi \otimes \mathbf{e_\Phi} + \mathbf{e}_z \otimes \mathbf{e_Z} \ . \tag{13}$$

We prescribed the values of the undeformed inner radius R_i and outer radius R_o to be 40 mm and 50 mm, respectively.

For an incompressible material, the deformation is isochoric and is subjected to the kinematic constraint $\det \mathbf{F}^e = 1$. Using Eqs. (3) and (13), this kinematic constraint reduces to

$$\frac{dr}{dR} = \frac{\theta^3 R}{r} \ . \tag{14}$$

Integrating this kinematic constraint leads to:

$$r - r_i = \int_{R_i}^{R} \theta^3 R \, \mathrm{d}R \ . \tag{15}$$

The fiber direction in the cylindrical tube model was prescribed to be in the circumferential direction, i.e., $(f, s, n) = (\Phi, R, Z)$, and the material parameters of the Fung's law in Eq. (5) were given values $C = 0.1$kPa, $b_f = 20$, $b_s = 3$ and $b_{fs} = 3$.

The shear stresses $\sigma_{rz} = \sigma_{r\theta} = \sigma_{\phi z} = 0$ and the normal stresses σ_{rr}, $\sigma_{\phi\phi}$, σ_{zz} are functions of only the radial position r when the cylindrical tube is inflated. Thus, the equlibrium equation (9) is reduced to a scalar equation:

$$\frac{d\sigma_{rr}}{dr} + \frac{\sigma_{rr} - \sigma_{\phi\phi}}{r} = 0 \ . \tag{16}$$

With a prescribed internal pressure p_i and zero external pressure, the boundary conditions at the tube inner and outer radius are

$$\sigma_{rr}|_{r=r_i} = -p_i \ , \qquad \sigma_{rr}|_{r=r_o} = 0 \ . \tag{17a, b}$$

Integrating the equilibrium equation (16) and incorporating the boundary conditions leads to the following integral equation for the internal pressure,

$$p_i = -\int_{r_i}^{r_o} \frac{\sigma_{rr} - \sigma_{\phi\phi}}{r} \, \mathrm{d}r \ . \tag{18}$$

Combining Eqs. (3) - (8) and (13), we can rewrite Eq. (18) in the following form,

$$\begin{aligned} p_i = -\frac{1}{2}C \int_{r_i}^{r_o} \exp Q \Bigg\{ b_3 \left(\frac{\theta^8 R^4}{r^4} - \frac{\theta^4 R^2}{r^2} \right) - \\ b_1 \left(\frac{r^4}{R^4\theta^4} - \frac{r^2}{R^2\theta^2} \right) \Bigg\} \frac{1}{r} \, \mathrm{d}r \ . \end{aligned} \tag{19}$$

However, integration of (19) requires knowledge of the dependency of r on R. This dependency is obtained through the integral form of the kinematic constraint in Eq. (15).

Equations (15) and (19), together with the kinetics of growth and reverse growth in Eqs. (10) - (12) form an initial value problem. We prescribed $\tau_g = \tau_{rg} =$ 1s, $\gamma_g = \gamma_{rg} = 1$, $\lambda_{h1} = \lambda_{h2} = 1.3$, $\theta_{\max} = 2$ and $\theta_{\min} = 1$ for the parameters describing the kinetics of growth and reverse growth in the cylindrical tube model. The unknowns for this set of equations are the growth multiplier θ and the inner radius of the tube in the current configuration r_i. Since the elastic fiber stretch λ_e is a function of the radial coordinate R in the undeformed configuration, the growth multiplier θ depends on the radial position and may vary across the thickness.

To mimic the hemodynamic loading of the heart, we prescribed a sawtooth time-periodic pressure-time curve for inner pressure $p_i(t)$ (Figure 2).

We assumed that the timescale for growth is significantly larger than the time scale for hemodynamic loading, which allows us to separate the time scales between growth and hemodynamics. As such, we locally update the growth multiplier θ using explicit-time integration only at the end of each loading cycle. Within

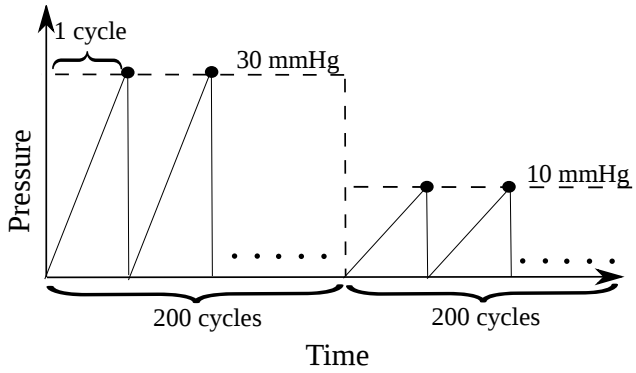

Fig. 2: Prescribed cyclical hemodynamics load p_i of the cylindrical tube model

each cycle, Eqs. (15) and (19), with θ treated as a constant, are recast into a nonlinear root finding problem for a scalar function defined as

$$\mathscr{F}(r_i) = p_i + \frac{1}{2}C\int_{r_i}^{r_o} \exp Q\left\{b_3\left(\frac{\theta^8 R^4}{r^4} - \frac{\theta^4 R^2}{r^2}\right) - b_1\left(\frac{r^4}{R^4\theta^4} - \frac{r^2}{R^2\theta^2}\right)\right\}\frac{1}{r}\,\mathrm{d}r = 0\,, \tag{20}$$

where

$$r(R) = r_i + \int_{R_i}^{R} \theta^3 R\,\mathrm{d}R\,. \tag{21}$$

The explicit-time integration of Eq. (3) is implemented in MATLAB (The MathWorks, Inc) to solve the initial value problem. The MATLAB functions "fsolve" and "quad" are used to solve Eqs. (20) and (21), and evaluate the integrals, respectively.

4 Growth and Reverse Growth of a Human Left Ventricle

After testing our model on an idealized cylindrical tube model, we applied our model to a more realistic left ventricular geometry of a normal human subject.

The construction of the left ventricle is shown in Figure 3. Specifically, the left ventricular epicardial and endocardial surfaces were reconstructed from magnetic resonance images (MRI) by manual segmentation using MeVisLab (MeVis Medical Solutions AG, Bremen, Germany) (Figure 3(a) and (b)). A hexahedral mesh consisting of 3456 trilinear elements was generated in the ventricular wall bounded by the epicardial and endocardial surfaces using the meshing software TrueGrid (XYZ Scientific Application, Livermore, CA, USA) (Figure 3(c)). Following Legrice et al. (1997), we prescribed a rule-based local myofiber orientation field in the ventricular wall, where the myofiber helix angle (measured with respect to the counter-clockwise circumferential direction) varies linearly from $-60°$ at the epicardial wall to $60°$ at the endocardial wall (see Figure 3(d)).

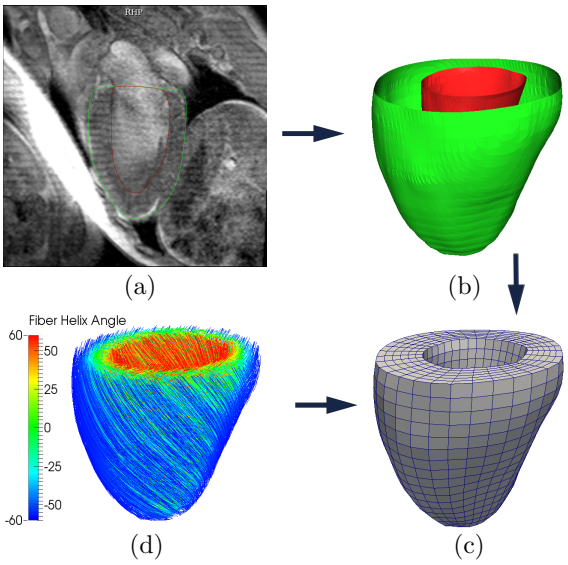

Fig. 3: Construction of the human left ventricle finite element model: (a) segmentation of the MRI, (b) reconstruction the endocardial (red) and epicardial (green), (c) construction of the finite element mesh and (d) assignment of rule-based myofiber orientation - streamlines follow fiber direction and are color coded with fiber helix angle.

Similar to the cylindrical tube model, the elastic deformation of the ventricle is described using Fung's constitutive equation given in Equation (5). The material parameters are $C = 0.195$kPa, $b_f = 24.63$, $b_s = 9.63$ and $b_{fs} = 8.92$, which correspond to the values defined in the human modeling study by Wenk et al. (2012). For the growth parameters, we chose $\tau_g = \tau_{rg} = 1$ s and $\gamma_g = \gamma_{rg} = 1$.

The homeostatic range of the elastic stretch at which neither growth nor reverse growth occurs ($\lambda_{h1} \leq \lambda_e \leq \lambda_{h2}$) was chosen as the range of the elastic stretch under a nominal end-diastolic pressure $\bar{P} = 10$ mmHg applied to the endocardial surface.

Figure 4 shows the prescribed pressure-time variation to simulate growth and reverse growth in the human left ventricle. A cyclical high end-diastolic pressure $\bar{P}^+ = 30$ mmHg was applied successively to induce stretch-driven growth. The high pressure loading was applied until growth has converged to a biological equilibrium state. Thereafter, a low end-diastolic pres-

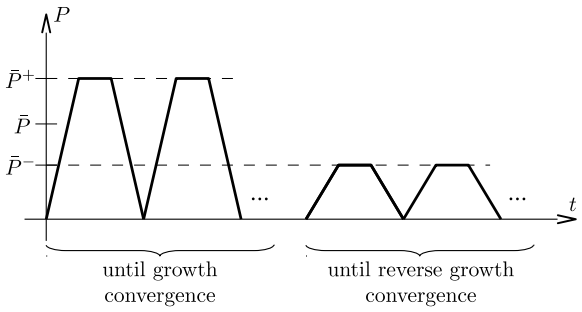

Fig. 4: Loading curve for the left ventricle. In practice we computed five loading-unloading cycles with high pressure, and five with low pressure. Every growth step lasts one characteristic time of the growth model.

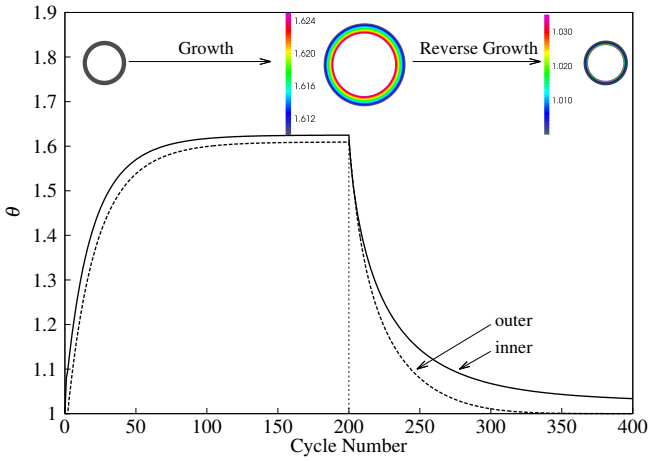

Fig. 5: Growth multiplier θ at the inner and outer surfaces as a function of the cycle number. Cross section of the unloaded cylindrical tube are shown in the inset at cycles 0, 200 and 400. Color denotes growth multiplier θ in cycles 200 and 400.

sure $\bar{P}^- = 2$ mmHg was applied cyclically to induce reverse growth and shrink the ventricular geometry until reverse growth had converged to a second biological equilibrium state.

Similar to the idealized cylindrical tube model, we hypothesize that the timescale of a cardiac cycle and the timescales of growth or reverse growth are separable. This implies that we update the growth multiplier θ only at peak pressure in each cycle.

5 Results

5.1 Growth and Reverse Growth of a Cylindrical Tube

Figure 5 shows the evolution of the growth multiplier θ at the inner and outer surfaces R_i and R_o under the imposed hemodynamic pressure loading (Figure 2). For the first 200 cycles at which the pressure p_i was elevated, the growth multiplier θ increased monotonically at a decreasing rate and approached steady-state with different values at the inner and outer surfaces of the tube. Because the steady-state values lay between the maximum and minimum permissible values of the growth multiplier i.e. $\theta_{\min} = 1$ and $\theta_{\max} = 2$, the vanishing growth rates at steady-state at both inner and outer surfaces are the outcome of $\lambda_e \to \lambda_{h2}$ as the elastic stretch approached its homeostatic value. In a similar fashion, the growth multiplier θ decreased after 200 cycles in response to the reduced pressure p_i, and approached a steady-state value as $\lambda_e \to \lambda_{h1}$.

Figure 6 shows the effects of (a) growth and (b) reverse growth on the relationship between pressure p_i and the tube internal radius r_i. During growth, both the internal radius of the unloaded tube (i.e. r_i at $p_i = 0$) and the entire p_i - r_i relationship shifted to the right and asymptotically approached the first equilibrium state at which $\lambda_e = \lambda_{h2}$. During reverse growth, the inner radius and the p_i - r_i relationship shifted to the left and asymptotically approached the second equilibrium state at which $\lambda_e = \lambda_{h1}$

We note that the $p_i - r_i$ relationship at the equilibrium state after reverse growth ($N = 400$) is different from the original one before the onset of growth i.e. at cycle = 1 (dotted line). This is because of the existence of differential growth across the cylindrical tube wall. Therefore, residual stresses, i.e., internal stresses in the unloaded tube, were generated as a result.

Figure 7 shows the variation of normal residual stresses σ_{rr}, $\sigma_{\phi\phi}$ and σ_{zz} across the tube wall at (a) the "fully grown" steady-state, and at (b) the "fully shrunk" steady-state. Although residual stresses in the "fully shrunk" steady-state are substantially smaller than that in the "fully grown" steady-state, they all share the same features. Specifically, the circumferential normal stress $\sigma_{\phi\phi}$ varies from negative at the inner wall indicating compression to positive at the outer wall indicating tension. By comparison, the longtitudinal normal stress σ_{zz} is negative across the entire tube wall. A compressive σ_{zz} arises largely because the prescribed plane deformation of the model in Eq. (13) is not compatible with the isotropic growth deformation prescribed in Eq. (2). Therefore, in order to maintain the plane deformation prescribed in Eq. (13), the tube must be elastically compressed in its longitudinal direction when growth occurs. On the other hand, the normal radial stress σ_{rr} satisfies the boundary conditions in Eq. (17) with $p_i = 0$, and is relatively small when compared to the other two stress components.

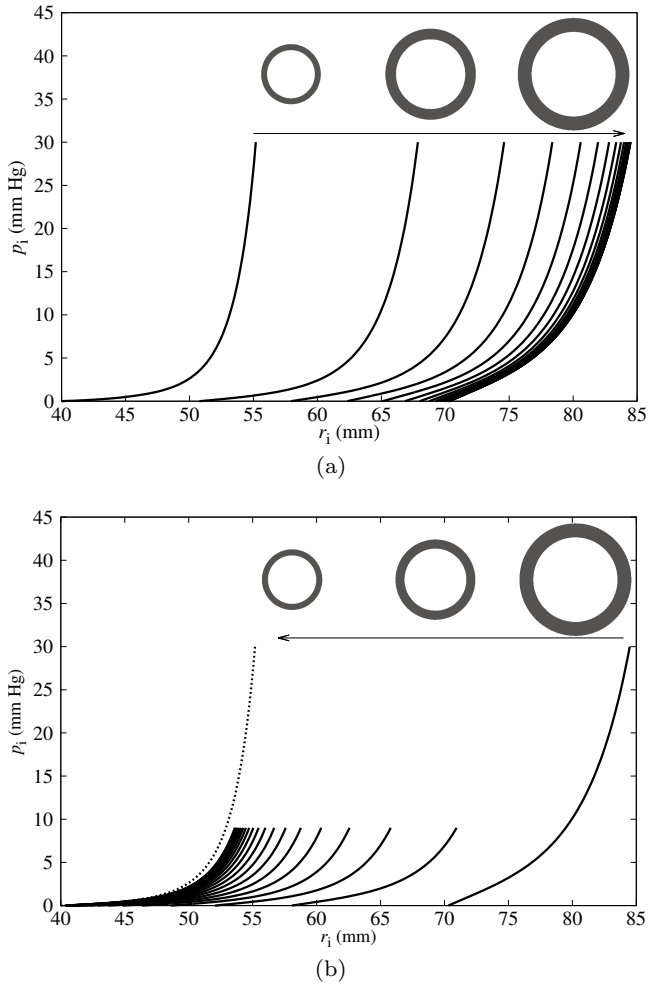

Fig. 6: Internal pressure p_i vs inner radius r_i at every 10th cycle in (a): cycles 1 - 200 during growth (inset: unloaded cylindrical cross section at cycles 1, 20, 200) and (b) cycles 200 - 400 during reverse growth (inset: unloaded cylindrical cross section at cycles 200, 220, 400). Dotted line: p_i vs r_i at first cycle.

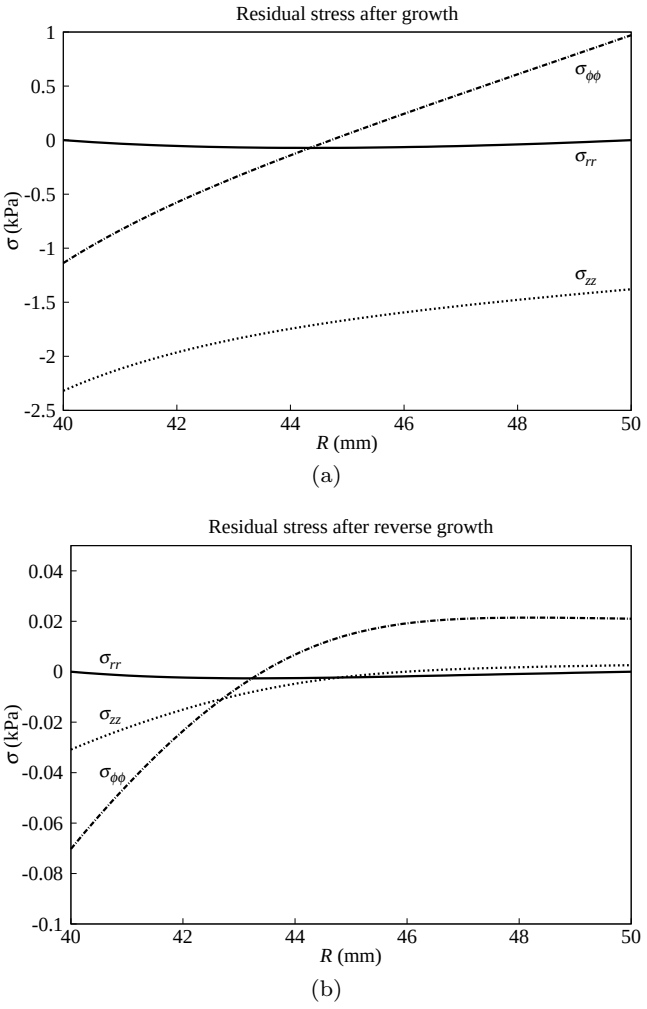

Fig. 7: Residual normal stresses in the circumferential ($\sigma_{\phi\phi}$), radial (σ_{rr}) and longitudinal (σ_{zz}) directions vs referential radial position R at the beginning of (a) cycle 201 and (b) cycle 400 with $p_i = 0$.

5.2 Growth and Reverse Growth of a Human Left Ventricle

For the nominal pressure $\bar{P} = 10$ mmHg, the range of elastic stretch in the left ventricle lay between lower and upper limits of 1.05 and 1.15, respectively. These limits were used to set the homeostatic range of elastic stretch, i.e., $\lambda_{h1} = 1.05$ and $\lambda_{h2} = 1.15$ in the reversible growth constitutive model (see Sections 2.3 and 2.4).

Figure 8 shows the pressure-volume relationship of the left ventricle model under the prescribed loading given in Figure 4. The curves display similar features as the pressure-radius relationship of the idealized cylindrical tube model in Figure 6, where the entire pressure-volume relationship shifted to the right under a high end-diastolic pressure loading of $\bar{P}^+ = 30$ mmHg (Figure 8a), and shifted to the left under a low end-diastolic pressure of $\bar{P}^- = 2$ mm Hg (Figure 8b). Correspondingly, the unloaded LV cavity volume also increased and decreased (both by ~ 5 ml) in response to the high and low end-diastolic pressure loading, respectively. Similar to the cylindrical tube model, the pressure-volume relationship in the final cycle of reverse growth is not identical to the initial one before the onset of growth although their unloaded left ventricular cavity volume are close to one another.

Figure 9 shows the evolution of the left ventricular geometry color-coded with the growth multiplier θ field as a result of growth and a subsequent reverse growth. In the figure, the ventricle increased slightly in size with growth (Figure 9b), corresponding to 20% increase in left ventricular volume, and shrinked longtitudinally as

a result of reverse growth (Figure 9d), corresponding to a recovery of the initial ventricular volume. Growth is largely heterogeneous in which the endocardial (inner) wall exhibits larger growth when compared to the epicardial (outer) wall. This result is consistent with observations from the cylindrical tube model (see Figure 5). The apical region exhibits a little shrinkage (i.e. $\theta < 1$) during growth (Figure 9b) and more substantial shrinkage during reverse growth (Figure 9d). During growth, the ventricle grows and becomes more spherical. This is in agreement with clinical observations during eccentric hypertrophic growth and implies that the apex is mechanically unloaded. The reduced apical stretch initiates negative growth in the apical region even during a global overload.

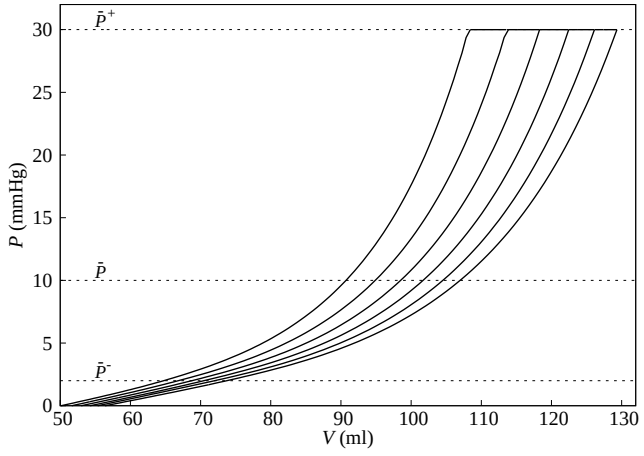

(a)

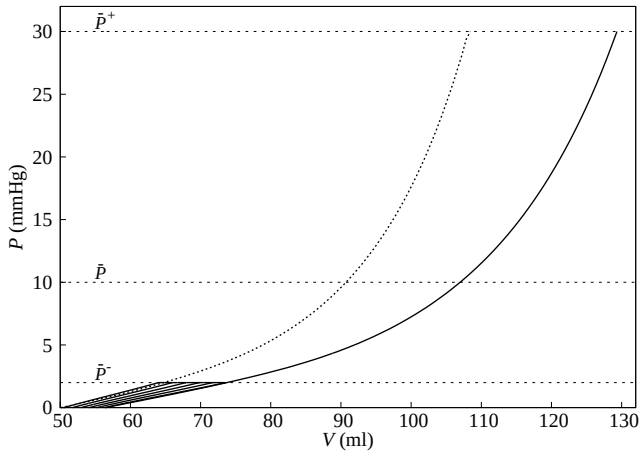

(b)

Fig. 8: Evolution of the pressure-volume relationship of the left ventricle during (a) growth and (b) reverse growth. The first and last cycle of the pressure-volume relationship in (a) is also shown in (b) as solid and dotted lines, respectively. Refer to text for definition of $\bar{P}^-$, $\bar{P}$ and $\bar{P}^+$.

Figure 10 shows the evolution of the elastic myofiber stretch λ_e field as a result of growth and reverse growth. The regional profile of the elastic fiber stretch is similar to the profile of the growth multiplier (Figure 9) as the stretch is the driving mechanism for growth. During growth and reverse growth, the elastic fiber stretch becomes more homogeneous across the ventricular wall. Specifically, the range of elastic fiber stretch changed from $\lambda_e = 1.02 - 1.22$ to $\lambda_e = 1.04 - 1.18$ after growth (between cycle 1 - 5) and from $\lambda_e = 0.97 - 1.10$ to $\lambda_e = 1.01 - 1.07$ during reverse growth (between cycle 6 - 10).

6 Discussions

We have established a constitutive model for reversible growth based on the frameworks of irreversible stretch-driven growth by Göktepe et al. (2010b) and the multiplicative decomposition of deformation gradient into an elastic and "growth" component by Rodriguez et al. (1994). Specifically, we have established the first model with a homeostatic equilibrium range for soft tissue growth that is analogous to hard tissue growth in bone. This homeostatic equilibrium zone is often referred to as a "lazy" zone in bone (Frost 2003).

Using this constitutive model, we have constructed a semi-analytical solution based on an idealized cylindrical tube model and a numerical solution based on a realistic model of an MRI-reconstructed human left ventricle. We have shown that in these models, growth and reverse growth were induced by a change in peak hemodynamic load where the global effects of growth and reverse growth were manifested by a rightward and leftward shift of the entire pressure-volume relationship, respectively (Figures 6 and 8). We have also shown that the resultant elastic myofiber stretch field after growth and reverse growth was more homogeneous in the left ventricle.

6.1 Compatibility with experimental studies and clinical observations of ventricular remodeling

Our model and results are consistent with a wide body of clinical observations and experimental studies. In terms of ventricular remodeling, the model predictions are consistent with the classical concept of eccentric hypertrophy arising from volume overload (e.g. mitral regurgitation): during volume overloading, on the cellular level, myocytes in patients with ischemic cardiomyopathy were found to be lengthened through the serial addition of sarcomeres (Gerdes et al. 1992). On the organ scale, hearts of these patients became enlarged and more spherical (Cohn et al. 2000). Our

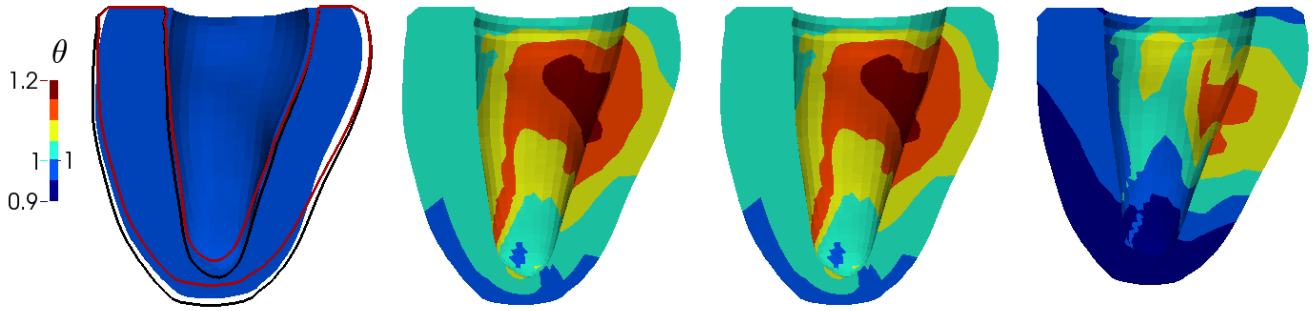

(a) Before growth (Cycle 1) (b) After growth (Cycle 5) (c) Before reverse growth (Cycle 6) (d) After reverse growth (Cycle 10)

Fig. 9: Evolution of the unloaded geometry and growth multiplier θ field of the left ventricle as a result of growth and reverse growth. Geometries are of the same scale. Black and red line in (a) correspond to the geometry outline of (b) and (d), respectively. Note: (b) and (c) are identical since no growth or reverse growth occurred between these 2 time points.

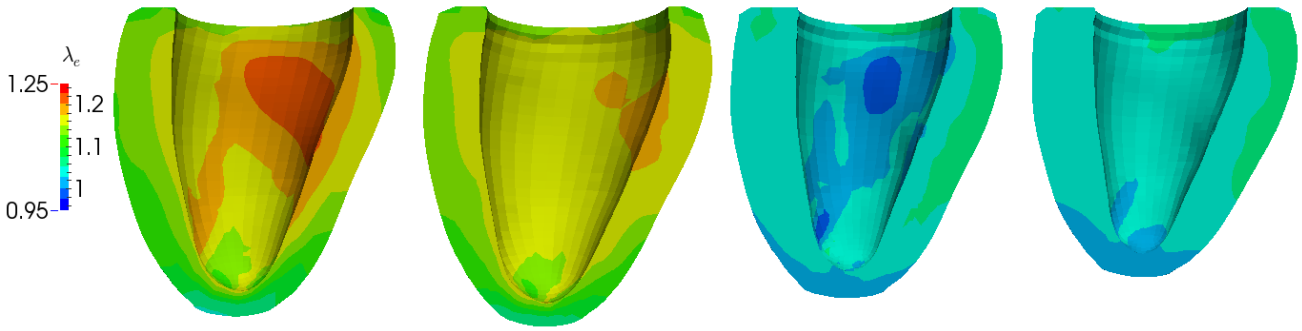

(a) Before growth (Cycle 1) (b) After growth (Cycle 5) (c) Before reverse growth (Cycle 6) (d) After reverse growth (Cycle 10)

Fig. 10: Evolution of elastic myofiber stretch λ_e in the left ventricle as a result of growth and its reversal. Geometries are of the same scale.

model predicts the increase of sphericity in response to overload. In particular, we observed that eccentric growth tends to unload the apex, in which we observed negative growth, even during overload. In contrast to the original hypothesis by Grossman et al. (1975) that end-diastolic myofiber stress is the myocardial growth stimulant during volume overload, Omens (1998) suggested end-diastolic myofiber strain as the growth stimulant. Specifically, Omens (1998) showed that the end-diastolic myofiber strain in rats induced with volume overload was normalized by 6 weeks during volume-overload hypertrophy whereas end-diastolic myofiber stress remained elevated during this time period. The global effects of an increase in preload associated with volume-overload hypertrophy are observed clinically in the form of pressure-volume relationship. For example, with the development of chronic mitral valve regurgitation, the entire pressure-volume relationship in patients has frequently been observed to shift rightwards (Gaasch and Meyer 2008) in a manner that is qualitatively consistent with our models' prediction.

6.2 Compatibility with experimental studies and clinical observations of ventricular reverse remodeling

In contrast to myocardial growth and remodeling which has been the subject of intense mathematical model development (Göktepe et al. 2010b; Kerckhoffs et al. 2012; Kroon et al. 2009), there are few, if any, mathematical models that describe the reverse of growth and remodeling. However, the phenomenon of reverse growth has increasingly been observed both experimentally and clinically, especially in response to recent clinical interventions. The original concept of reverse remodeling was

spawned by the effects of left ventricular assist devices in normalizing end-diastolic pressure-volume relationship in patients with end-stage cardiomoypathy (Levin et al. 1995) that has been frequently observed in clinical practice (Burkhoff et al. 2006; Drakos et al. 2007; Ambardekar and Buttrick 2011). In particular, prolonged unloading of the left ventricular pressure (and volume) after device implanation (Figure 1 in Burkhoff et al. (2006)) led to a decrease in left ventricular volume, and a concurrent leftward shift in the end-diastolic pressure-volume relationship (Figure 2 in Levin et al. (1995)). Microscopically, these effects were accompanied by a decrease in myocyte size (Figure 2 in Madigan et al. (2001)). The fact that these effects were typically not seen in the right ventricle, where the hemodynamics loading remained elevated (Burkhoff et al. 2006), provided perhaps the strongest support of a causal relationship between a reduction in ventricular loading and the reversal of remodeling.

Reverse remodeling was also observed in other clinical interventions that are associated with a reduction in ventricular loading, albeit less frequently than with left ventricular assist devices. For example, a significant reduction in the left ventricular size (up to 50%) was observed in patients that underwent bioinjection treatment with Algiysl-LVR, a calcium-sodium-alginate hydrogel proprietary to Lonestar Heart, Inc (Lee et al. 2013). In previous studies, the bioinjection treatment was associated with a decrease in end-diastolic myofiber stress (Wenk et al. 2011) and a leftward shift in end-diastolic pressure-volume relationship (Wall et al. 2006), which both suggest a decrease in the elastic myofiber stretch. Reverse geometrical remodeling of the left ventricle was also observed after mitral valve repair which decreases preload (Brinke et al. 2010). Given that the experiment by Omens (1998) strongly suggests an elevated elastic myofiber strain as the stimulant of ventricular remodeling, it is also very plausible that the reverse holds, i.e., a reduction in elastic myofiber strain initiates reverse ventricular remodeling. These observations are the basis of our proposed constitutive model for reversible strain-driven growth, which we have shown to be able to reproduce the clinically and experimentally observed trend of the end-diastolic pressure-volume relationship during ventricular reverse remodeling.

6.3 Compatibility with experimental studies and clinical observations on growth-induced residual stress

Since non-homogeneous growth generates incompatibility that must be accommodated elastically, differential growth in the left ventricle in response to a non-homogenous strain field will generate residual stresses, i.e., stresses in the unloaded state. The residual stress fields generated through our constitutive model in the idealized cylindrical model at maximal growth (Figure 7) are consistent with other models utilizing the same cylindrical geometry (Rodriguez et al. 1994; Guccione et al. 1991). In Guccione et al. (1991), the residual stress field was the result from prescribing a "cut" cylindrical model as a stress-free reference configuration whereas in Rodriguez et al. (1994), the residual stress field was the result of stress-modulated differential growth. Consistent with these models, the circumferential stress varies transmurally from compressive (at the endocardial wall) to tensile (at the epicardial wall). We also showed that our model predicts an increase in residual stresses during ventricular remodeling and a subsequent decrease in residual stresses during reverse ventricular remodeling (Figure 7).

The effects of pathological ventricular remodeling and reverse remodeling on residual stress and strain are still unclear given the paucity of experiments that studied these effects. To the best of our knowledge, the only two studies on the effects of residual stresses and strain due to ventricular remodeling is the study by Omens et al. (1998) on aging rat heart (i.e., physiological remodeling), and Taber and Chabert (2002) on developing embryonic chick heart. In the former, the opening angle of the left ventricular equatorial ring after a radial cut was found to decrease during aging, while in the latter, the opening angle in embryonic chick heart was found to decrease as a result of pressure overload. It is not entirely clear whether the reduction in opening angle in the experiment by Omens et al. (1998) was accompanied by a change in tissue stiffness, as besides differential growth, a change in tissue stiffness will also have an effect on the opening angle (Taber and Chabert 2002). The impact on the opening angle as a result of a change in tissue stiffness can be illustrated by considering a hypothetical case in which the tissue becomes infinitely compliant (i.e. have zero stiffness) during ventricular remodeling. In this limiting state, the left ventricle will be in a "stress-free" state even with finite growth and correspondingly, the opening angle will be zero. As such, future experiments to test our model prediction on the effects on residual stresses and strain due to ventricular remodeling and reverse remodeling should separate the effects arising from differential growth and a change in material properties.

6.4 Limitation the model

Our proposed model of reversible growth and remodeling does have limitations. One key limitation is the fact that we have neglected the effects on myocardial ma-

terial properties due to remodeling and reverse remodeling. In the experiments by Omens (1998), volume-overload ventricular remodeling in rats was found to be associated with an increase in the mechanical stiffness of the myocardial tissues. A change in mechanical properties would not only have a confounding effect on the residual strain measured using the "opening angle" of radially cut slices of the left ventricle (as expounded in the previous paragraph), but also on the end-diastolic pressure-volume relationship. Another limitation of our model (as with other existing volumetric growth models) is that it cannot distinguish between a change in the number of myocytes (i.e. hyperplasia or dysplasia) from a change in cell size (i.e. hypertrophy or atrophy) (Taber 2001).

7 Conclusions

In conclusion, we have established a reversible strain-driven growth model and have shown that the proposed model can qualitatively reproduce many experimental and clinical observations of ventricular remodeling and reverse remodeling. Specifically, we have shown that our model prediction on the effects of end-diastolic pressure-volume relationship due to growth and reverse growth are compatible with clinical and experimental observations. We had also shown that our model prediction on the residual stress fields in an idealized cylindrical model are similar to that in other non-identical models, namely, a model with stress-modulated growth and a model using a longtitudinally cut cylinder as a stress-free configuration. Although our proposed model can qualitatively reproduce clinical and experimental observations of ventricular remodeling and reverse remodeling, more experiments will be necessary to test the basis of our proposed constitutive model and its predictions.

Acknowledgements This work was supported by NIH grants R01-HL-077921 and R01-HL-118627 (J.M. Guccione); K25-NS058573-05 (G. Acevedo-Bolton); NSF grants 0952021 and 1233054 (E. Kuhl); and Marie-Curie international outgoing fellowship within the 7th European Community Framework Program (M. Genet).

References

Ambardekar, A. V. and Buttrick, P. M. (2011), "Reverse remodeling with left ventricular assist devices: a review of clinical, cellular, and molecular effects.", *Circ. Hear. Fail.* **4**(2), 224–33.

Ambrosi, D., Ateshian, G. A., Arruda, E. M., Cowin, S. C., Dumais, J., Goriely, A., Holzapfel, G. A., Humphrey, J. D., Kemkemer, R., Kuhl, E., Olberding, J. E., Taber, L. A. and Garikipati, K. (2011), "Perspectives on biological growth and remodeling.", *J. Mech. Phys. Solids* **59**(4), 863–883.

Brinke, E. A., Klautz, R. J., Tulner, S. A., Verwey, H. F., Bax, J. J., Delgado, V., Holman, E. R., Schalij, M. J., van der Wall, E. E., Braun, J., Versteegh, M. I., Dion, R. A. and Steendijk, P. (2010), "Clinical and functional effects of restrictive mitral annuloplasty at midterm follow-up in heart failure patients.", *Ann. Thorac. Surg.* **90**(6), 1913–20.

Burkhoff, D., Klotz, S. and Mancini, D. M. (2006), "LVAD-induced reverse remodeling: basic and clinical implications for myocardial recovery.", *J. Card. Fail.* **12**(3), 227–39.

Cohn, J. N., Ferrari, R. and Sharpe, N. (2000), "Cardiac remodelingconcepts and clinical implications: a consensus paper from an international forum on cardiac remodeling", *J. Am. Coll. Cardiol.* **35**(3), 569–582.

Drakos, S. G., Terrovitis, J. V., Anastasiou-Nana, M. I. and Nanas, J. N. (2007), "Reverse remodeling during long-term mechanical unloading of the left ventricle.", *J. Mol. Cell. Cardiol.* **43**(3), 231–42.

Frost, H. M. (2003), "Bone's mechanostat: a 2003 update.", *Anat. Rec. A. Discov. Mol. Cell. Evol. Biol.* **275**(2), 1081–101.

Gaasch, W. H. and Meyer, T. E. (2008), "Left ventricular response to mitral regurgitation: implications for management.", *Circulation* **118**(22), 2298–303.

Gerdes, A. M., Kellerman, S. E., Moore, J. A., Muffly, K. E., Clark, L. C., Reaves, P. Y., Malec, K. B., McKeown, P. P. and Schocken, D. D. (1992), "Structural remodeling of cardiac myocytes in patients with ischemic cardiomyopathy", *Circulation* **86**(2), 426–430.

Göktepe, S., Abilez, O. J. and Kuhl, E. (2010a), "A generic approach towards finite growth with examples of athlete's heart, cardiac dilation, and cardiac wall thickening", *J. Mech. Phys. Solids* **58**(10), 1661–1680.

Göktepe, S., Abilez, O. J., Parker, K. K. and Kuhl, E. (2010b), "A multiscale model for eccentric and concentric cardiac growth through sarcomerogenesis.", *J. Theor. Biol.* **265**(3), 433–42.

Grossman, W., Jones, D. and McLaurin, L. P. (1975), "Wall stress and patterns of hypertrophy in the human left ventricle.", *J. Clin. Invest.* **56**(1), 56–64.

Guccione, J. M., McCulloch, A. D. and Waldman, L. K. (1991), "Passive material properties of intact ventricular myocardium determined from a cylindrical model.", *J. Biomech. Eng.* **113**(1), 42–55.

Kerckhoffs, R. C. P. (2012), "Computational modeling of cardiac growth in the post-natal rat with a strain-based growth law.", *J. Biomech.* **45**(5), 865–71.

Kerckhoffs, R. C. P., Omens, J. and McCulloch, A. D. (2012), "A single strain-based growth law predicts concentric and eccentric cardiac growth during pressure and volume overload.", *Mech. Res. Commun.* **42**, 40–50.

Klepach, D., Lee, L. C., Wenk, J. F., Ratcliffe, M. B., Zohdi, T. I., Navia, J. a., Kassab, G. S., Kuhl, E. and Guccione, J. M. (2012), "Growth and remodeling of the left ventricle: A case study of myocardial infarction and surgical ventricular restoration.", *Mech. Res. Commun.* **42**, 134–141.

Kroon, W., Delhaas, T., Arts, T. and Bovendeerd, P. (2009), "Computational modeling of volumetric soft tissue growth: application to the cardiac left ventricle.", *Biomech. Model. Mechanobiol.* **8**(4), 301–9.

Lee, E. H. (1969), "Elastic-Plastic Deformation at Finite Strains", *J. Appl. Mech.* **36**(1), 1–6.

Lee, L. C., Wall, S. T., Klepach, D., Ge, L., Zhang, Z., Lee, R. J., Hinson, A., Gorman, J. H., Gorman, R. C. and Guccione, J. M. (2013), "Algisyl-LVR with coronary artery bypass grafting reduces left ventricular wall stress and improves function in the failing human heart.", *Int. J. Cardiol.* **168**(3), 2022–2028.

Legrice, I. J., Hunter, P. J. and Smaill, B. H. (1997), "Laminar structure of the heart: a mathematical model.", *Am. J. Physiol.* **272**(5 Pt 2), H2466–76.

Levin, H., Oz, M., Chen, J., Packer, M., Rose, E. and Burkhoff, D. (1995), "Reversal of chronic ventricular dilation in patients with end-stage cardiomyopathy by prolonged mechanical unloading", *Circulation* **91**(11), 2717–2720.

Madigan, J. D., Barbone, A., Choudhri, A. F., Morales, D. L., Cai, B., Oz, M. C. and Burkhoff, D. (2001), "Time course of reverse remodeling of the left ventricle during support with a left ventricular assist device.", *J. Thorac. Cardiovasc. Surg.* **121**(5), 902–8.

Omens, J. H. (1998), "Stress and strain as regulators of myocardial growth.", *Prog. Biophys. Mol. Biol.* **69**(2-3), 559–72.

Omens, J. H., Vaplon, S. M., Fazeli, B. and Mcculloch, A. D. (1998), "Left Ventricular Geometric Remodeling and Residual Stress in the Rat Heart", *J. Biomech. Eng.* **120**, 715–719.

Opie, L. H., Commerford, P. J., Gersh, B. J. and Pfeffer, M. A. (2006), "Controversies in cardiology.", *Lancet* **367**(9519), 1315; author reply 1315–6.

Rausch, M. K., Dam, A., Göktepe, S., Abilez, O. J. and Kuhl, E. (2011), "Computational modeling of growth: systemic and pulmonary hypertension in the heart.", *Biomech. Model. Mechanobiol.* **10**(6), 799–811.

Rodriguez, E. K., Hoger, A. and Mcculloch, A. D. (1994), "Stress-dependent finite growth in soft elastic tissues.", *J. Biomech.* **27**(4), 455–467.

Taber, L. A. (1995), "Biomechanics of Growth, Remodeling, and Morphogenesis", *Appl. Mech. Rev.* **48**(8), 487–545.

Taber, L. A. (2001), "Biomechanics of cardiovascular development", *Annu. Rev. Biomed. Eng.* **3**, 1–25.

Taber, L. A. and Chabert, S. (2002), "Theoretical and experimental study of growth and remodeling in the developing heart.", *Biomech. Model. Mechanobiol.* **1**(1), 29–43.

Wall, S. T., Walker, J. C., Healy, K. E., Ratcliffe, M. B. and Guccione, J. M. (2006), "Theoretical impact of the injection of material into the myocardium: a finite element model simulation.", *Circulation* **114**(24), 2627–35.

Wenk, J. F., Eslami, P., Zhang, Z., Xu, C., Kuhl, E., Gorman, J. H., Robb, J. D., Ratcliffe, M. B., Gorman, R. C. and Guccione, J. M. (2011), "A novel method for quantifying the in-vivo mechanical effect of material injected into a myocardial infarction.", *Ann. Thorac. Surg.* **92**(3), 935–41.

Wenk, J. F., Klepach, D., Lee, L. C., Zhang, Z., Ge, L., Tseng, E. E., Martin, A., Kozerke, S., Gorman, J. H., Gorman, R. C. and Guccione, J. M. (2012), "First evidence of depressed contractility in the border zone of a human myocardial infarction.", *Ann. Thorac. Surg.* **93**(4), 1188–93.